Octopolar Chromophores Based on Donor- and Acceptor-Substituted 1,3,5-Tris(phenylethynyl)benzenes: Impact of meta -Conjugation on the Molecular and Electronic Structure by Means of...

ARTICLE *in* THE JOURNAL OF PHYSICAL CHEMISTRY B · OCTOBER 2006

Impact Factor: 3.3 · DOI: 10.1021/jp0627269 · Source: PubMed

4 AUTHORS, INCLUDING:

Juan Casado
University of Malaga
227 PUBLICATIONS **3,688** CITATIONS
SEE PROFILE

Gunther Hennrich
Universidad Autónoma de Madrid
52 PUBLICATIONS **945** CITATIONS
SEE PROFILE

Juan Teodomiro López Navarrete
University of Malaga
335 PUBLICATIONS **5,249** CITATIONS
SEE PROFILE

Octopolar Chromophores Based on Donor- and Acceptor-Substituted 1,3,5-Tris(phenylethynyl)benzenes: Impact of *meta*-Conjugation on the Molecular and Electronic Structure by Means of Spectroscopy and Theory

María Moreno Oliva,[†] Juan Casado,[†] Gunther Hennrich,*[,‡] and Juan T. López Navarrete*[,†]

Departamento de Química Física, Universidad de Málaga, Campus de Teatinos s/n, Málaga 29071, Spain, and Departamento de Química Orgánica, Universidad Autónoma de Madrid, Cantoblanco, Madrid 28049, Spain

Received: May 4, 2006; In Final Form: July 17, 2006

The molecular and electronic structures of a series of all-*meta*-substituted phenylacetylene mesitylenes peripherally substituted with donor or acceptor (D−A) groups are studied. The impact of *meta*- and *para*-substitution patterns is also analyzed by employing Raman and optical spectroscopies in conjunction with theoretical calculations. Outer phenyl rings display a partial quinoid character induced by two different motifs: (i) outer phenyls → triple bond charge transfer for the cases where these phenyls are substituted with electron-donors; (ii) double electron withdrawing effect in the molecules with the peripheral phenyls substituted with electron acceptors. A moderate tuning of the optical gap is observed in agreement with the partial blockade of π-electron conjugation exerted by the *meta* disposition. The orbital structure of the compounds partially preserves that of the mesitylene group showing extra-conjugation due to the addition of the arms, so that conjugation is not entirely obstructed but partially impeded in the ground electronic state (i.e., electron occupied orbitals). As for the excited states, the low-lying energy empty orbitals offer better conditions for full conjugation over the whole molecular scaffold. Interesting optical properties such as overlapping centers along the lowest energy optical excitations and enhanced optical transparency with importance for the application of these materials in optoelectronics have been justified on the basis of the electronic structure. A greater degree of quinoidization, and more allowed π-electron delocalization, over the entire molecule is recognized in the case of linear phenylacetylenes substituting in *para* positions the central core.

I. Introduction

Nonlinear optical (NLO) materials have attracted much interest because of their potential applications in optoelectronic technology. In particular organic molecules are very suitable in this field owing to their fast electronic responses to external stimuli, ease and flexibility of chemical design, lightweighting materials, good processability in devices, etc.[1] In this context, two-dimensional (2D) octopolar molecules, with 1,3,5-triamino-2,4,6-trinitrobenzene (TATB) being the prototypical example, are shown to exhibit second-order NLO features similar to those of their one-dimensional (1D) D−π-A dipolar homologues, overcoming their intrinsic limitations.[2] For example, 1D molecules suffer from poor transparency−efficiency tradeoff, their dipolar nature induces the formation of centrosymmetric crystal with inactive second harmonic generation responses, and phase-matching conditions cause only a fraction of the microscopic response to be preserved at the macroscopic scale. On the contrary, 2D octopolar architectures show an improved transparency−efficiency ratio, give rise to noncentrosymmetric arrangements, and present large off-diagonal β tensor components that warrant a large macroscopic second harmonic generation response.[3] Following the example of TATB, a common way to design NLO-active octopolar molecules is to synthesize noncentrosymmetrically substituted C_3-symmetric systems. Acetylenic systems constitute among octopolar NLO chromophores those with the highest second-order polarizabilities known so far.[4] We have recently reported on the fabrication of a simple device for second-order nonlinear optics based on liquid cristalline 1,3,5-tris(alkynyl)benzene derivatives with octopolar symmetry. In the bulk phase, these molecules self-assemble in a noncentrosymmetric fashion which allows for efficient second-harmonic generation from the solid sample device.[5]

Apart from of the NLO activity, a different aspect of all-*meta*-substituted aromatics is of fundamental interest, especially in the context of dendritic systems. It has been postulated by various research groups that the electronic states in *meta*-branched phenylacetylene dendrimers are located on the linear acetylenic arms, under the assumption that *meta*-conjugation blocks electronic delocalization in the ground-electronic states but offers an excellent condition for electron coupling in the excited states.[6] The explanation given for this phenomenon consists of a reconfiguration of the π-orbitals responsible for the electronic communication of the subunits, which supposedly adopt a cumulenic structure in the excited state.[7] This hypothesis is backed up by various experimental and theoretical studies.[8] Such behavior, generating a gradient of charge distribution over the whole system, is of great practical importance due to directed charge-transfer (CT) processes occurring in the dendritic system. This geometry-dependent electronic coupling modulates the energy transfer in the dendritic system and/or the NLO-activity in the presence of an intense electric field.[9]

This work deals with a series of peripherally donor- or acceptor-substituted phenylacetylenic arms coupled via the 1, 3, and 5 positions to mesitylene acting as the central core. The main tool to probe ground electronic state features will be

* To whom correspondence should be addressed.
[†] Universidad de Málaga.
[‡] Universidad Autónoma de Madrid.

10.1021/jp0627269 CCC: $33.50
Published on Web 09/01/2006

SCHEME 1: Synthesis of 1,3,5-Tris(alkynyl)mesitylenes (PAMes) and Chemical Structures of the Studied Compounds

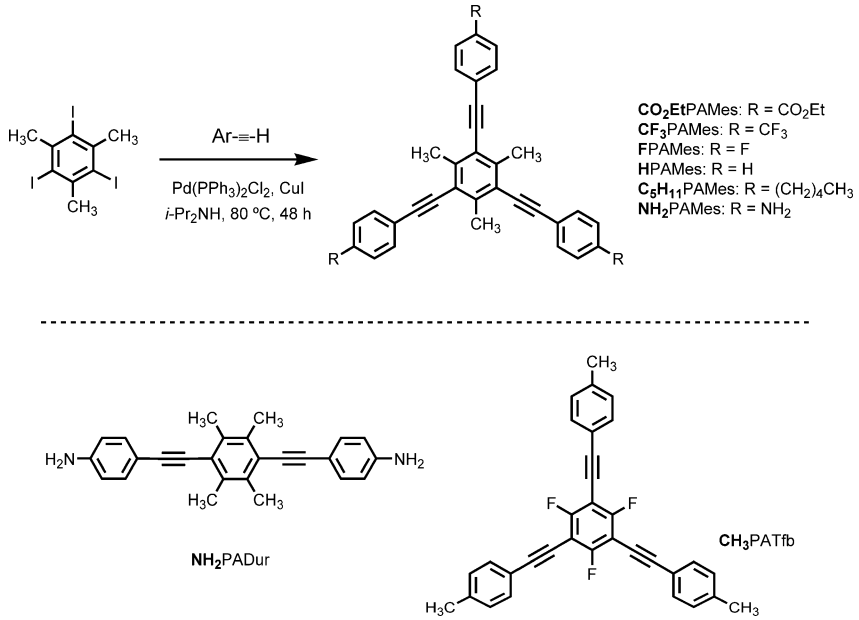

Raman spectroscopy. Vibrational Raman spectroscopy is well suited for studying the electronic coupling between covalently connected conjugated moieties.[10] This originates from the important enhancement of the Raman activity for those vibrational modes that vibronically couple the electronic structure of the ground electronic state and the first accessible dipole-allowed excited state.[11] In this sense the Raman wavenumbers as a function of the substitution pattern can delineate the impact and extent of conjugation in these chromophores. The second part of the paper deals with the study of the electronic structure by UV−vis electron absorption and emission spectra. The photophysical properties are inspected, allowing predictions of the electronic features of both the ground and the excited states. The understanding of the underlying structure−property relationships will be used to evaluated the electronic structure in relationship with the NLO activity and, on the other hand, with the electronic impact of *meta*-conjugation of acetylenic arms in comparison with *para*-substitution and with the inversion of the substitution pattern. All the experimental data in this paper are supported by theoretical calculations in the framework of the density functional theory for ground-state properties and time-dependent density functional theory for excited states.

II. Synthesis

All 1,3,5-tris(alkynyl)mesitylenes (PAMes) and the trifluorobenzene compound (**CH**$_3$PAPfb) as well as the linear 1,4-bis(alkynyl)durene derivative (**NH**$_2$PADur) are readily obtained via standard Sonogashira cross-coupling of 1,3,5-triiodomesitylene with the respective *p*-phenylethynyl compounds as described previously for **H**PAMes, **CF**$_3$PAMes, and **C**$_5$**H**$_{11}$-PAMes (Scheme 1).[12]

1,3,5-Tris((4-fluorophenyl)ethynyl)-2,4,6-trimethylbenzene (FPAMes). Purification by column chromatography (20:1 Hex−EtOAc) and final recrystallization from cyclohexane gave pure **F**PAMes as colorless crystals. Yield: 243 mg; 51%. Mp: 168−170 °C. ^{1}H NMR: δ = 7.57−7.48 (m, 6 H), 7.11−7.00 (m, 6 H), 2.71 (s, 9 H). ^{13}C NMR: δ = 162.5 (d, J = 249.8 Hz), 141.9, 134.5, 133.2, 119.6, 115.5, 96.3, 86.5, 20.2; EI$^+$-HRMS: found, 474.1597; calcd for $C_{33}H_{21}F_3$, 474.1595. R_f = 0.57 (20:1 Hex−EtOAc).

1,3,5-Tris[((4-ethoxycarbonyl)phenyl)ethynyl)]-2,4,6-trimethylbenzene (**CO**$_2$**EtPAMes).** Purification by column chromatography (10:1 Hex−EtOAc) and final recrystallization from *i*-PrOH gave pure **CO**$_2$EtPAMes as an off-white solid. Yield: 268 mg; 42%. Mp: 134−138 °C. ^{1}H NMR: δ = 8.04 (d$_{AB}$, J = 8.2 Hz, 6 H), 7.60 (d$_{AB}$, J = 8.2 Hz, 6 H), 4.40 (q, J = 7.0 Hz, 6 H), 2.75 (s, 9 H), 1.42 (t, J = 7.0 Hz, 9 H). ^{13}C NMR: δ = 166.0, 142.9, 131.3, 130.0, 129.6, 128.0, 121.1, 97.0, 89.5, 61.2, 20.4, 14.3. MALDI-HRMS: found, 636.2506; calcd for $C_{42}H_{36}O_6$, 636.2522. R_f = 0.59 (5:1 Hex−EtOAc).

1,3,5-Tris[(4-amino(L)phenyl)ethynyl)]-2,4,6-trimethylbenzene (**NH**$_2$**PAMes).** Purification by column chromatography (20:1 CH_2Cl_2−MeOH) and final recrystallization from acetonitrile gave pure **NH**$_2$PAMes as a yellow solid. Yield: 326 mg; 70%. Mp: 196 °C. ^{1}H NMR: δ = 7.37 (d$_{AB}$, J = 8.8 Hz, 6 H), 6.66 (d$_{AB}$, J = 8.8 Hz, 6 H), 3.83 (s, 6 H), 2.71 (s, 9 H). ^{13}C NMR: δ = 146.6, 140.7, 132.7, 121.6, 114.8, 113.1, 97.8, 85.1, 20.2. FAB$^+$-HRMS: found, 466.2278; calcd for $C_{33}H_{28}N_3$, 466.2275. R_f = 0.86 (20:1 CH_2Cl_2−MeOH).

1,3,5-Tris[(4-methylphenyl)ethynyl]-2,4,6-trifluorobenzene (**CH**$_3$**PATfb).** Purification by column chromatography (10:1 Hex−EtOAc) and final recrystallization from cyclohexane gave pure **CH**$_3$PATfb as colorless crystals. Yield: 303 mg; 64%. Mp: 184 °C. ^{1}H NMR: δ = 7.48 (d$_{AB}$, J = 8.1 Hz, 6 H), 7.19 (d$_{AB}$, J = 8.1 Hz, 6 H), 2.39 (s, 9 H). ^{13}C NMR: δ = 163.4, 160.0, 139.4, 132.8, 130.2, 128.1, 119.1, 99.9, 73.8, 20.8. EI$^+$-HRMS: found, 474.1587; calcd for $C_{33}H_{21}F_3$, 474.1595. R_f = 0.48 (20:1 Hex−EtOAc).

1,4-Bis[(4-aminophenyl)ethynyl]-2,3,5,6-tetramethylbenzene (**NH**$_2$**PADur).** Purification by column chromatography (20:1 CH_2Cl_2−MeOH) and final recrystallization from nitromethane gave pure **NH**$_2$PADur as a dark yellow solid. Yield: 233 mg; 64%. Mp: >300 °C. ^{1}H NMR: δ = 7.29 (d$_{AB}$, J = 8.3 Hz, 4 H), 6.69 (d$_{AB}$, J = 8.3 Hz, 4 H), 5.05 (bs, 4 H), 2.46 (s, 12 H). ^{13}C NMR: δ = 149.9, 135.6, 133.3, 124.3, 115.0, 111.8, 100.5, 86.6. EI$^+$-HRMS: found, 364.1948; calcd for $C_{26}H_{24}N_2$, 364.1939. R_f = 0.70 (20:1 CH_2Cl_2−MeOH).

III. Raman Spectra and Molecular Structure

Figure 1 compares the FT-Raman and FT-Infrared spectra of **F**PAMes in the solid state. According to the prediction of the group theory for the C_{3h} point group of symmetry, those bands emerging from totally symmetric modes (i.e., A′ species)

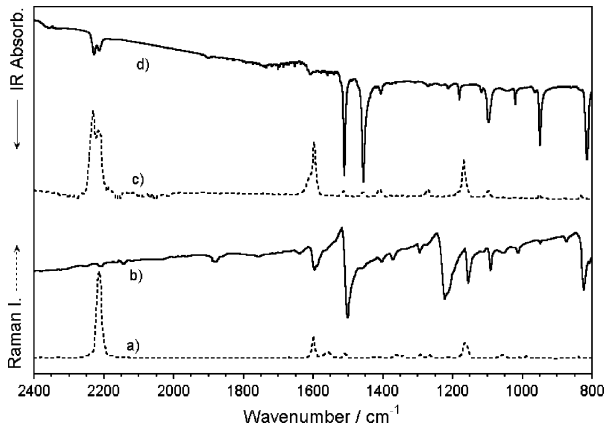

Figure 1. FT-IR (bold line) and FT-Raman (dashed line) of (a and b) **F**PAMes and of (c and d) **CH**$_3$PATfb .

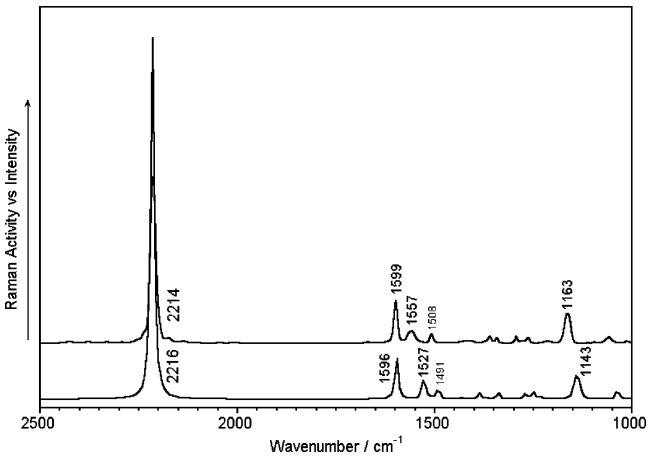

Figure 2. Comparison of the DFT//B3LYP/6-31G** (bottom) and of the experimental (top) Raman spectra of **F**PAMes.

are active in Raman and silent in infrared. Considering that in these compounds the Raman intensity distribution is governed by vibronic coupling (i.e., the A term of the Albrecht theory), only the A′ totally symmetric among the Raman-active modes are expected to be intense or very intense. Therefore, at a first sight, those vibronically enhanced modes intense in Raman should be inactive in infrared. Consequently, for the C_{3h} planar geometry both spectra should be *complementary*. A comparison of these spectra reveals that there are some features, at the same frequency, that are weak in the IR and very intense in Raman (i.e., see the IR/Raman bands at 2203 cm^{-1} as a prototypical example). A reasonable argument to solve this apparent contradiction is the rupture of the C_{3h} symmetry (i.e., distortion of the planarity), a fact that can explain this vibrational effect and another important features of the electronic spectra in section IV. This behavior is also typical of vibrations associated with local modes in which local symmetry conditions, rather than the whole molecular symmetry, might apply. A prototypical case is the ν(CH) vibrations in the region around 3000 cm^{-1}. In our molecules this case must be discarded, on one hand, because the IR/Raman complementarity is found in an extensive spectral region and, on the other hand, because of the ν(CC) nature of the discussed bands.

Before we attempt to understand the evolution of the Raman spectra with the substitution pattern, an assignment of the main Raman lines must be first considered. Therefore, one is helped with the microscopic normal modes (i.e., vibrational eigenvectors) as deduced by the DFT//B3LYP/6-31G** simulation of the Raman spectrum of the representative **F**PAMes case. A comparison between the experimental and theoretical Raman spectra for this molecule is offered in Figure 2, while Figure 3 depicts the vibrational modes associated with the most important bands.

III.a. Raman Assignment. The agreement between theoretical and experimental spectra is quite satisfactory. Moreover, both spectra show a surprisingly simple appearance with a small number of Raman bands, seemingly in contradiction with the large number of Raman-active modes predicted by group theory. The intervention of an effective coupling of some particular vibrations to the electronic structure, or vibronic interaction due to the existence of a π-electron system, leads to those vibrational modes spreading along an *alternating* C−C/C═C/C≡C bond sequence to excite the electron−phonon mechanism, deriving in a strong enhancement of their Raman activity.[11] This selective intensity enhancement of totally symmetric modes is the main reason for the spectral simplicity.

The most intense band of the Raman spectrum of **F**PAMes is measured at 2214 cm^{-1} (calcd: 2216 cm^{-1}) and emerges from a stretching mode of the acetylenic spacer, or ν(C≡C). The medium-intensity band at 1599 cm^{-1} (calcd: 1596 cm^{-1}) corresponds to the symmetric stretching vibration of the CC bonds of the external benzene groups in parallel disposition relative to the acetylene groups. According to its eigenvector, the same vibration is recognized in the core at 1557 cm^{-1} (calcd: 1527 cm^{-1}) but now coupled with a deformation vibration of this central ring. A very clear CCC deformation vibration of the core underlies in the experimental band at 1163 cm^{-1} (calcd: 1143 cm^{-1}), slightly coupled with the same mode in the outer benzenes. Finally, the weak band at 1508 cm^{-1} (calcd: 1491 cm^{-1}) turns now to be completely located at the peripheral rings owing to a combination of CC stretching and CH deformation modes.

III.b. Structure−Spectra Relationships. Figure 4 shows the FT-Raman spectra of the studied compounds. Owing to the π-electronic inactivity of the methyl groups, hexamethylbenzene is an adequate system for comparing the evolution of the Raman spectra upon substitution of the mesitylene with the phenylacetylenic arms. The Raman spectrum of hexamethylbenzene shows an intense and characteristic peak at 1585 cm^{-1} with the same dynamic description of that around 1555 cm^{-1} in our series. The 20 cm^{-1} downshift of this band is in agreement with the CC bond elongation experienced by the central six-membered ring (i.e., from 1.395/1.403 Å to 1.411/1.417 Å in **NH**$_2$PAMes) as a consequence of the electron withdrawal effect of the acetylenic substituents.[10] These Raman lines scarcely move in the series, except for **CO**$_2$EtPAMes to 1544 cm^{-1} indicating the strong electron-withdrawing effect of the **CO**$_2$-Et-phenylacetylene moiety. Figure 5 summarizes the main DFT//B3LYP/6-31G** theoretical bond lengths of some representative examples.

As for the Raman band of the external benzenes, a wavenumber upshift upon D−A substitution is observed; thus, it evolves from 1599 cm^{-1} in **H**PAMes to 1605 cm^{-1} in **NH**$_2$-PAMes or to 1606 cm^{-1} in **CO**$_2$EtPAMes. This behavior is in accordance with the strengthening of the CC bonds mainly involved in the dynamic of this mode (i.e., the ones parallel to the triple bond) since they vary from 1.393 Å in in **H**PAMes to 1.392/1.390 Å in **NH**$_2$PAMes or to 1.391/1.388 Å in **CF**$_3$PAMes at the DFT//B3LYP/6-31G** level. In both cases, this finding might be highlighting the following: (i) a quinoidization of this benzene ring as a result of a partial donor (NH$_2$) → acceptor (C≡C) charge transference in **NH**$_2$PAMes; (ii) a charge density withdrawing over this ring caused by the local effect of two acceptor moieties in **CO**$_2$EtPAMes.

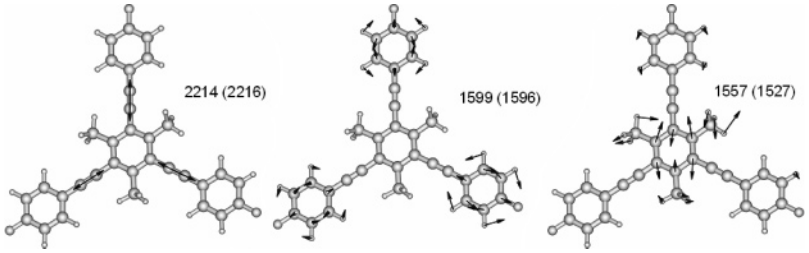

Figure 3. DFT//B3LYP/6-31G** vibrational eigenvectors associated with the most important Raman lines (theoretical values in parentheses) of **F**PAMes.

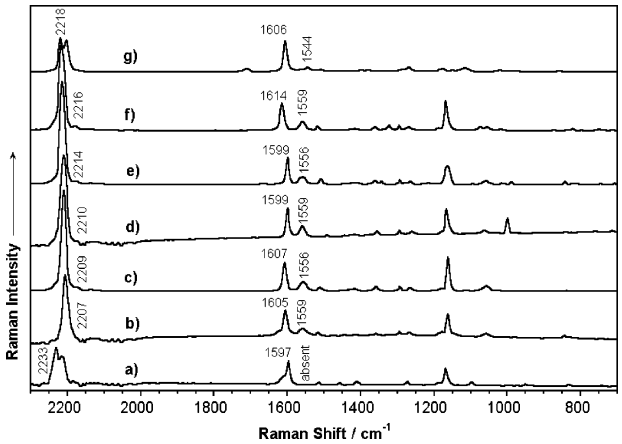

Figure 4. FT-Raman spectra of the studied compounds: (a) **CH**$_3$-PATfb; (b) **NH**$_2$PAMes; (c) **C**$_5$H$_{11}$PAMes; (d) **H**PAMes; (e) **F**PAMes; (f) **CF**$_3$PAMes; (g) **CO**$_2$EtPAMes.

TABLE 1: Polarization of the $C_{central}$≡C_{periph} Bonds from ^{13}C NMR Spectra

substituent	σ_{Hammet}	$\delta(C_{central})$/ppm	$\delta(C_{peripheric})$/ppm	$\Delta\delta$/ppm	$\nu_{(C\equiv C)}$
CO$_2$EtPAMes	0.45	97.0	89.5	7.5	2218
CF$_3$PAMes	0.32	96.3	88.9	7.4	2216
FPAMes	0.06	96.3	86.5	9.8	2214
HPAMes	0	97.4	86.9	10.5	2210
C$_5$H$_{11}$PAMes	−0.17	97.6	86.4	11.2	2209
NH$_2$PAMes	−0.66	97.8	85.1	12.7	2207

SCHEME 2: Schematic Representation of Charge Transfer and Cumulene Formation on NH$_2$PAMes

As for the ν(C≡C) modes at 2200 cm^{-1}, they show a different tend with respect to the above Raman bands; thus, a continuous upward displacement of this peak is observed from 2207 cm^{-1} in **NH$_2$**PAMes to 2218 cm^{-1} in **CO$_2$**EtPAMes. Theoretical data do not provide a clear insight into the evolution of the C≡C bond lengths as they show a constant value of 1.217 Å, with the exception of **H**PAMes. The same tendency for the triple bond is noticed in the ^{13}C NMR spectra appointing the difference of the chemical shifts of the two carbon atoms of the acetylene group. This value can be related with the polarization of the triple bond[13] and changes continuously in the series from **CO$_2$**-EtPAMes to **NH$_2$**PAMes (see Table 1).

Assuming that the increased polarization of this bond contributes to the cumulenic structure (see Scheme 2), then the increasing contribution of this cumulene pattern in the amine derivative is in accordance with the lowest wavenumber of its ν(C≡C) Raman line (where the triple bond is expected to weaken upon cumulenization). Furthermore, this stresses the fact of a NH$_2$ → C≡C charge transfer to account for the quinoidization of this benzene ring.

III.c. *meta* vs *para* Substitution. The spectra of **NH$_2$**PADur and **NH$_2$**PAMes (i.e., *meta*) are displayed in Figure 6. The strong fluorescence clearly impacts the quality of the FT-Raman spectrum of **NH$_2$**PADur, although the features around 1550−1600 cm^{-1} can be measured at the expense of the ν(C≡C) Raman line obscured in the background. In line with the discussion in the above section, the 1605 → 1609 cm^{-1} upshift in **NH$_2$**PAMes → **NH$_2$**PADur might be understood by a gaining of quinoidal character (i.e., resulting from donor → acceptor charge transfer) in the outermost phenyl rings of the *para*-derivative (see Scheme 2). This experimental finding is supported theoretically by only a slight strengthening of the parallel bonds of these rings which are shortened by 0.001 Å.

The central core undergoes more noticeable changes on *meta* vs *para* substitution. The CC bonds parallel to the acetylene are considerably shortened by 0.011 Å, while the others lengthen by 0.002 Å (Figure 5). This description is consistent with a larger quinoidization of this ring in the *para*-derivative. Also the C≡C bond distances, although to a lesser extent owing to their intrinsic strength, are lengthened by 0.001 Å compatible with the gaining cumulenic character of the acetylene spacer. The Raman spectrum of 1,4-benzoquinone (i.e., prototypical case of *para*-quinoid molecule) shows two key bands at 1606 and 1587 cm^{-1} characteristic of the quinoidal structure. As a result, the quinoid/cumulene evolution of the structure detected in **NH$_2$**-PADur leads to the evolution of a new band at 1595 cm^{-1} forming with the above feature at 1609 cm^{-1} the typical two-bands pattern due to the quinoidization of the core. The Raman band at 1572 cm^{-1} is reminiscent of the benzene-like hexa-substituted core. The 1559 (*meta*) → 1572 (*para*) cm^{-1} displacement is interpreted as a consequence of the greater local withdrawal effect of three phenylacetylene groups in **NH$_2$**-PAMes versus two in **NH$_2$**PADur, i.e., a σ-inductive effect driven by the sp/sp^2 electronegative difference.

III.d. Inverting the Substitution Pattern. Here the FT-Raman spectra of **F**PAMes and that of an 3-fold analogue molecule in which the position of the three fluorine and methyl groups are interchanged resulting a molecule with an inverted substitution pattern, **CH$_3$**PATfb, are compared (Figure 1). First noticeable is the great weak/intense Raman/IR pattern observed in the whole mid-IR interval. In the case of **F**PAMes this Raman/IR comparison was especially successful for some particular bands (i.e., 2200 cm^{-1}) while for **CH$_3$**PATfb this comparison better holds for the whole range. This fact might outline the increased planarity in **CH$_3$**PATfb explicable by the reduced steric bulk of the fluorine substituents on the central benzene core compared to methyl groups. At the same time this planarization might justify two findings: (i) the almost complete suppression of the weak absorption bands around 330 nm due to planarity distortion as discussed in section IV.a; (ii) a slight 2/6 nm red-shift of the absorption/emission bands is observed on **F**PAMes → **CH$_3$**PATfb also in agreement with

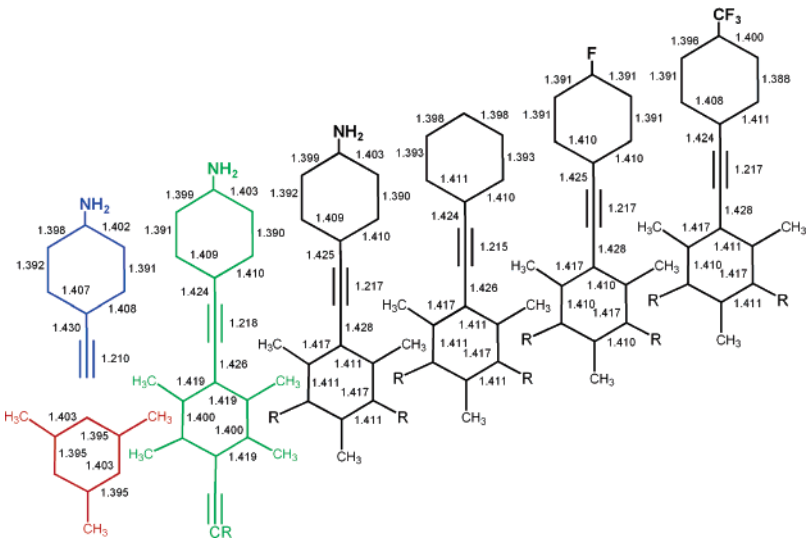

Figure 5. DFT//B3LYP/6-31G**-optimized skeletal CC bond lengths for some phenylacetylenic compounds and their building blocks. Only a representative part of each molecule is shown. Key: blue/red, isolated units; green, **NH**$_2$PADur.

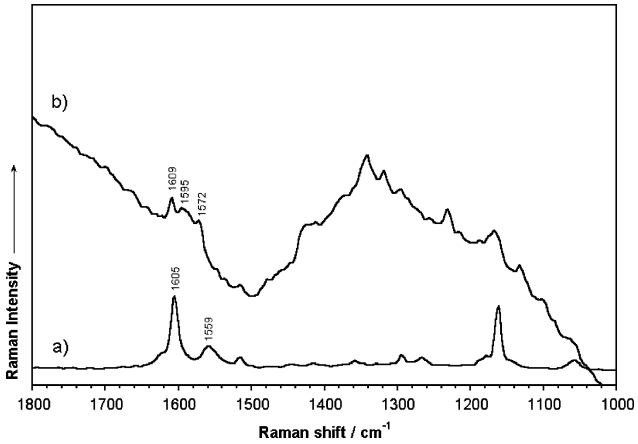

Figure 6. Comparison of the solid-state FT-Raman spectra of (a) **NH**$_2$-PAMes and (b) **NH**$_2$PADur.

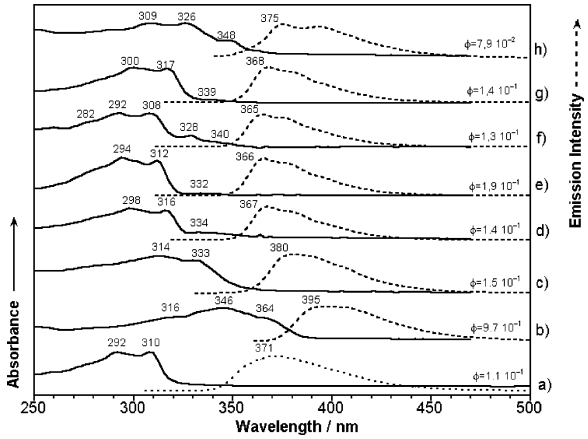

Figure 7. UV−vis absorption and emission spectra of the studied compounds in dichloromethane: (a) **CH**$_3$PATfb; (b) **NH**$_2$PADur; (c) **NH**$_2$PAMes; (d) **C**$_5$**H**$_{11}$PAMes; (e) **H**PAMes; (f) **F**PAMes; (g) **CF**$_3$-PAMes; (h) **CO**$_2$**Et**PAMes.

the slight HOMO−LUMO gap narrowing predicted by DFT//B3LYP/6-31G** theory (Figure 8).

As for the Raman spectra, the ν(C≡C) Raman line in **CH**$_3$-PATfb is upshifted and splits in two components relative to **F**PAMes. The higher frequency for this band is in accordance with the theoretical strengthening of the triple bonds (i.e., 1.215 Å in **CH**$_3$PATfb and 1.217 Å in **F**PAMes). The slight downshift of the line at 1597 cm^{-1} in **CH**$_3$PATfb relative to the same in **F**PAMes also agrees with the slight weakening of the bonds of the outermost benzenes that are parallel to the acetylene groups (i.e., 1.389/1.392 Å in **CH**$_3$PATfb and 1.391/1.391 Å in **F**PAMes). However, the band at 1556 cm^{-1} in **F**PAMes is missing in its inverted homologue. The averaged −0.006 Å CC bond shortening of the central phenyl ring in **CH**$_3$PATfb might push this band to higher energies (see Figure S1, Supporting Information). On the other hand, this vibration in **F**PAMes is mechanically coupled with the vicinal methyl deformation vibrations (see Figure 3), an effect that likely disappears upon translation of the CH_3 groups from the core to the periphery thus contributing to the disappearance of the around 1550 cm^{-1} band. In this regard, a shoulder of the intense line at 1597 cm^{-1} at 1609 cm^{-1} is observed for **CH**$_3$PATfb. No clear insights into the alteration of the charge-transfer interactions, as outlined for the other compounds, can be drawn upon pattern inversion. In this regard, in/out position interchange of the methyl/fluorine groups does not provoke much change of the optical properties which might have their incidence from a synthetic point of view.

IV. Electronic Spectra and Electronic Structure

IV.a. Electronic Absorption Assignment. Figure 7 shows the absorption and emission spectra of all the compounds. Figure 8 displays the energy position of some representative frontier orbitals and their topologies. The absorption spectra are characterized by the presence of medium-weak bands around 330 nm, while the intense absorptions appear in the interval 290−320 nm. For **F**PAMes, TD-DFT calculations predict that the most intense theoretical features are two degenerated transitions at 323 nm (i.e., equally intense, $f = 1.033$); however, the lowest lying energy transition at 357 nm is predicted to have zero oscillator strength. Both theoretical transitions seemingly correspond with the symmetric/antisymmetric combinations of the dipolar moment transition arrangements during the HOMO-1 → LUMO, HOMO → LUMO+1, HOMO-1 → LUMO+1 and HOMO → LUMO promotions. In particular, the two transitions calculated at 323 nm are due to the following multielectron excitations: 0.42/−0.18 [HOMO-1 → LUMO], −0.42/+0.18 [HOMO → LUMO+1], +0.18/+0.42 [HOMO-1 → LUMO+1], +0.18/+0.42 [HOMO → LUMO]. The nonallowed transition at 357 nm is composed as follows: +0.43 [HOMO-1 → LUMO]

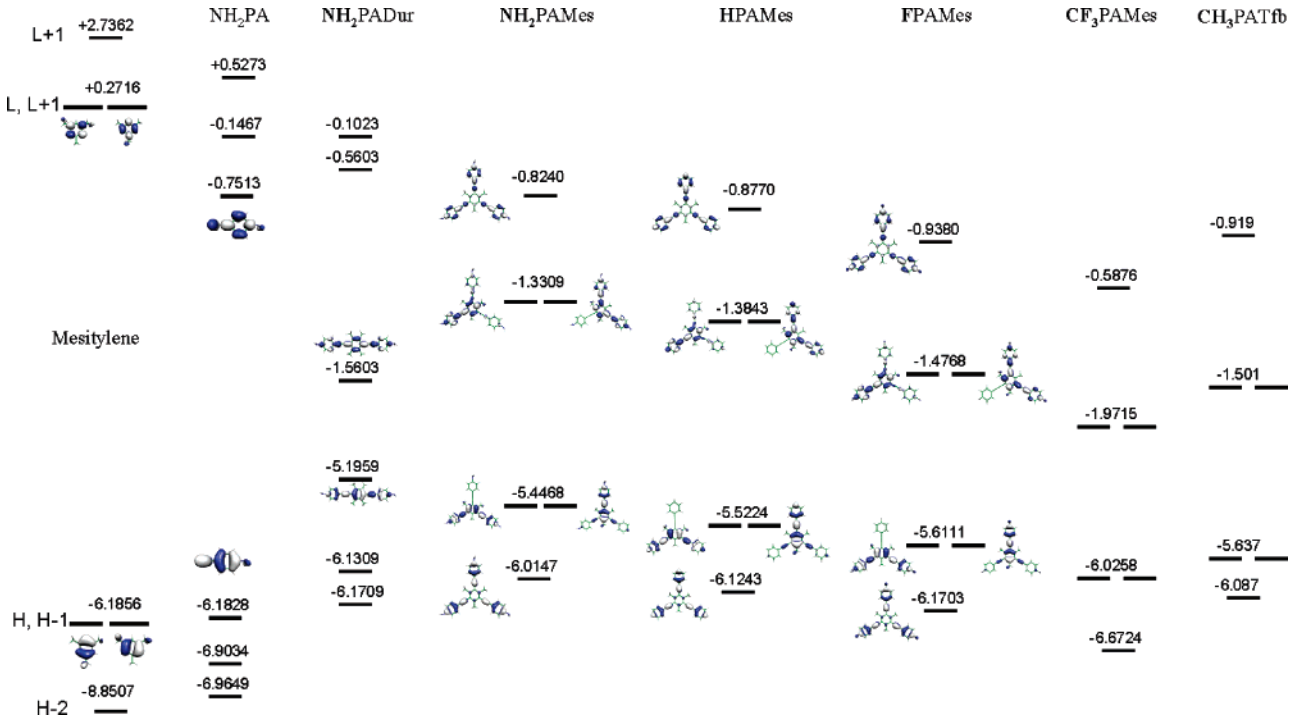

Figure 8. Schematic diagram with the B3LYP/6-31G** absolute energies and topologies of the frontier orbitals around the gap.

+ 0.43 [HOMO → LUMO+1] + 0.24 [HOMO-1 → LUMO+1] − 0.24 [HOMO → LUMO].

Taking into account that calculations were carried out by assuming a planar-C_{3h} symmetry, one would expect some distortions (i.e., see section III) from planarity to occur, especially in solution. This might give rise to the splitting of the degenerate transitions and the activation of the lowest energy excitation predicted to be prohibited. Finally, the medium band at 282 nm in **F**PAMes can be correlated with the double degenerate theoretical feature predicted at 290 nm, with oscillator strengths of 0.51, which are mainly composed of the HOMO-2 → HOMO and HOMO → LUMO+2 one-electron promotions.

IV.b. Electronic Structure−Optical Spectra Relationships. The electronic structure (i.e., orbitals around the gap) of the central mesitylene core is preserved to a certain extent upon 3-fold substitution. This means that the double degeneracy of the HOMO/HOMO-1 and LUMO/LUMO+1 orbitals observed in the octopolar compounds is reminiscent of the isolated mesitylene. In addition, the topologies of these orbitals in mesitylene and in the cores, roughly keep the same pattern, with extra contributions from the peripheral groups in the trialkynyl systems. This additional contribution originates from the direct combination of the HOMOs and LUMOs of the central mesitylene and of the arms (see Figure 8) which gives rise to the orbitals of the dendrimer-like samples.

The energetic disposition of these orbitals in the isolated elements and in the trigonal compounds differ substantially. In particular the HOMO energy is destabilized by around 0.7 eV on Mes → **NH$_2$**PAMes, while the LUMO is stabilized by 1.6 eV. This description is consistent with a greater electron delocalization between the arms through the core in the excited states involving the LUMO and LUMO+1. The lower and upper energy orbitals (i.e., HOMO-2 and LUMO+2) are mainly constituted by the acetylenic arms with small participation of the core. Conversely, substitution of the core with two **NH$_2$**PA arms in the *para* position leads to a more symmetric destabilization (i.e., by 1.1 eV)/stabilization (i.e., by 1.8 eV) of the HOMO/LUMO terms of the durene core stressing a better electron conjugation than in the *meta*-derivatives. Nonetheless, the LUMO orbitals in the *para*-compound still show preferential stabilization regarding the HOMOs. This might be justified by the existence of a sequence of bonding/nonbonding features in alternated bonds between the arms through the core. In the case of the HOMO of **NH$_2$**PADur, the wave function is partially cross-conjugated, giving rise to the smaller coupling. This effect is much more pronounced in the HOMOs of the trigonal compounds where an alternating sequence of bonding/nonbonding features along consecutive bonds cannot be established due to the presence of atoms in the core that do not participate in the molecular orbital anymore. As a consequence, the coupling is restricted, and the substituent effect on the HOMO is somewhat limited in the trigonal samples.

The finding of a greater stabilization of the LUMO is typical for extended conjugated systems revealing the electronic withdrawal effect of the acetylenic moiety in dependence of the peripheral substitution. In this context, the electrochemical properties of the samples have been investigated in the cathodic branch. It is well-known that *meta*-substituted phenylacetylene gives rise to irreversible reductions due to the blockade of electron delocalization over the central core.[10] Only for **CO$_2$Et**PAMes some electrochemical activity has been found in the cyclic voltammetry experiment (Figure 9) stressing the further increment of acceptor character inferred by the ester groups. In this case, the irreversible processes linked to **CO$_2$Et**PAMes are near the electrolyte decomposition region so that the voltammetric curve is scarcely resolved.

Peripheral substitution of H by alkyl or amine donor groups slightly shifts the maxima of the absorptions. These small changes are in agreement with similar stabilization of both occupied (i.e., 0.076 eV) and empty (−0.053 eV) frontier orbitals upon replacement of H by amine groups according to DFT//B3LYP/6-31G** theory. In the case of introduction of acceptors, there is a relatively moderate red-shift of the observed bands. Theory also predicts the narrowing of the optical gap in terms of the reduction of the difference between the occupied

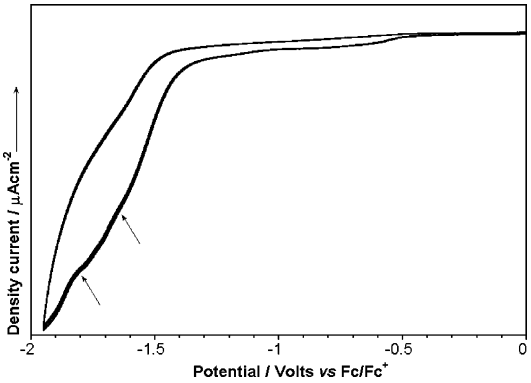

Figure 9. Cyclic voltammetry of **CO$_2$Et**PAMes in 0.1 M (TBA)PF$_6$ in dichloromethane. Scan rate: 100 mV/s. Working electrode: glassy carbon. Pseudoreference electrode: Ag wire. Counter electrode: Pt wire. Arrows denote irreversible processes.

and unoccupied molecular orbitals upon passing from **H**PAMes to **CF$_3$**PAMes (i.e., by 0.84 eV). Here, the HOMO → LUMO excitation implies a drifting and localization of the charge density from two of the three arms to the other, while the HOMO-1 → LUMO+1 transition carries out an expansion of it. As deduced from the orbital topologies, these excitations suppose a transference of the charge density between the arms in accordance with the strong oscillator strength of the allowed transitions. Accordingly, the energy difference between the HOMO/HOMO-1 and the LUMO/LUMO+1 apparently controls the optical gap.

Interestingly for these excitations, the central core and one arm constitute overlapping centers along the optical excitation. This is a molecular requirement for the appearance of nonlinear optical activity which has indeed been observed for the 1,3,5-tris(alkynyl)benzenes used in this study.[12] Let us therefore relate some of the data presented here with those already reported for the first hyperpolarizability of these octopolar compounds. In particular, data have been obtained for **H**PAMes ($(18 \pm 2) \times 10^{-30}$ esu), **C$_5$H$_{11}$**PAMes ($(32 \pm 2) \times 10^{-30}$ esu), and **CF$_3$**-PAMes ($(45 \pm 3) \times 10^{-30}$ esu) which nicely correlate with the theoretical prediction on the decreasing of the HOMO−LUMO gap, 4.1381 eV in **H**PAMes, 4.0954 eV in **C$_5$H$_{11}$**PAMes, and 4.0543 eV in **CF$_3$**PAMes, or by the decreasing of the experimentally recorded optical gap, 3.974 (3.735) eV in **H**PAMes, 3.924 (3.712) eV in **C$_5$H$_{11}$**PAMes, and 3.912 (3.658) eV in **CF$_3$**-PAMes (i.e., notice the existence of a $\beta \approx 1/\Delta E^2$ relationship where ΔE is approached, from a theoretical point of view, by the HOMO−LUMO gap or, experimentally, from the energy of the maximum of the lowest energy absorption bands).[14] Also beneficial for the nonlinear response is the finding associated with the weak intensity of the lowest energy band for these samples which is related with the critical requirement of optical transparency. In this regard, substitution with electron donor/acceptor peripheral groups modulates the optical gap by roughly 20 nm.

In summary, the structure−activity relationship established here from linear optical measurements can be directly related to the NLO behavior. This connection has also been confirmed by ab initio studies on related systems.[15] A general prediction of the second-order nonlinearities on the basis of the experimental and theoretical data presented in this work can be considered valid, addressing crucial parameters such as conjugation length, bond length alternation, donor−acceptor strength, CT character, molecular symmetry, etc. Though beyond the objective of this work, it is interesting to outline that as normal Raman scattering is connected to linear optical properties (one photon absorption and Raleigh scattering), the analysis of the second-order nonlinear optical response would be complemented with hyper-Raman scattering studies leading to get information on two photon absorption or (multiphoton) fluorescence phenomena. Hence the study of the hyper-Raman spectra of these NLO-active mesitylenes would likely give interesting results.[16]

IV.c. *meta* versus *para* Substitution. The electronic absorption spectrum of **NH$_2$**PADur displays bands bathochromically shifted by 30 nm compared with the absorption maxima of **NH$_2$**-PAMes, though their spectral profiles are quite similar (Figure 7). This reduction of the optical gap is well predicted by theory (0.5 eV) regarding the HOMO(HOMO-1)/LUMO(LUMO+1) energy difference. The HOMO and LUMO energies are destabilized/stabilized more symmetrically compared with **NH$_2$**-PAMes, emphasizing the greater impact of π-electron conjugation in both orbitals, in contrast to the case of the C_3-symmetric compounds. A more detailed description of this effect accounting for the molecular orbitals is presented in section IV.b.

IV.d. Emission Properties. All the emission spectra show similar spectral profiles. The appearance of 3−4 shoulders of the intense peak is likely due to vibronic structure. Provided that radiative emission proceeds through the $S_1 \rightarrow S_0$ channel, this S_1 state is mainly contributed by the LUMO/LUMO+1 orbitals which impose rigidity to the acetylenic spacer in a cumulenic-like structure and partial quinoidization of the external phenyls and central mesitylene. The combination of these two structural effects in the excited state probably enhances the vibronic coupling in the $S_1 \rightarrow S_0$ deactivation resulting in the structure of the emission band. In this scenario, for the S_1 state, a better conjugation through the whole system of the lone electron pairs of the nitrogen atoms of **NH$_2$**PAMes has been predicted which results in the greatest red-shift of the emission band observed in the series. For **NH$_2$**PADur, the emission feature is further displaced by +15 nm to the red compared to its homologue **NH$_2$**PAMes, highlighting the greater delocalization of the electron density through the core in a *para*-substituted system. The quantum yields measured for these molecules also stress the more efficient route for the $S_1 \rightarrow S_0$ deactivation in the *para*- system regarding the *meta*-substitution.

V. Conclusions

The molecular and electronic structures of a series of trigonal (C_3-symmetric all-*meta*-substituted) alkynylbenzenes conceived as octopolar chromophores have been studied. The novelty of the work consists of the completion of a series with donor and acceptor moieties of different strength in the periphery of the dendrimer-like system. The impact of the *meta*- and *para*-substitution patterns has been also analyzed. The investigation of the molecular structures is based on the dependence of the wavenumber of the Raman bands mainly involved in the π-conjugated path. The optical spectra, however, suppose the experimental basis for the analysis of the electronic structure. In all the cases, the experimental findings have been supported and correlated with quantum chemistry (DFT and TD-DFT).

It is recognized that the D−A character of the acetylene groups is divided into an inductive effect (through σ-bonds) and a mesomeric actuation (π-electron system). The existence of a partial quinoid character in the outer phenyl rings is due to the donor (periphery) → acceptor (triple bond) electron transfer mediated by the π-electron system. This mesomeric effect is compensated by the substitution with two electron acceptors, and a rather local inductive effect of the two withdrawal groups is the responsible of the moderate quinoidization of these rings in the peripherally acceptor substituted systems.

The electronic structure of these molecules has been interpreted from their constituting building blocks. A moderate tuning of the optical gap is observed in agreement with the partial blockade of π-electron conjugation in this all-*meta* disposition of the phenylacetylene groups. The orbital structure of the compounds partially preserves the features of the mesitylene group showing extra-conjugation due to the addition of the acetylene arms. This stresses the fact that conjugation is not entirely obstructed but partially impeded in the ground electronic state (i.e., HOMO orbitals). In this regard, the LUMO (LUMO+1) terms offer better conditions for conjugation over the entire π-system. Interesting optical properties (i.e., overlapping centers along the lowest energy optical excitations, or optical transparency) with importance in the application of these materials in optoelectronics have been justified on the basis of the electronic structure.

Greater quinoidization, and more extensive π-electron delocalization, over the entire molecule are deduced from the analysis of the Raman and optical spectra of the *para*-derivative compared to the *meta* case.

VI. Experimental and Theoretical Details

NMR data were collected on a Varian 300 MHz instrument. The chemical shifts are reported in ppm, and the coupling constants (*J*) are reported in Hz. $CHCl_3$ is referenced to the residual proton peak (5.32 ppm). Cyclic voltammetry data were collected on a Voltalab 40 potentiostat from Radiometer. Electrochemical data are reported vs Fc/Fc^+ in 0.1 M (TBA)-PF_6 in CH_2Cl_2 using a Ag wire (pseudoreference electrode), glassy carbon (working electronde), and a Pt foil (counter electrode). FT-Raman spectra were measured using an FT-Raman accessory kit (FRA/106-S) of a Bruker Equinox 55 FT-IR interferometer. A continuous-wave Nd:YAG laser working at 1064 nm was employed for excitation. A germanium detector operating at liquid-nitrogen temperature was used. Raman scattering radiation was collected in a backscattering configuration with a standard spectral resolution of 4 cm^{-1}. A total of 1000−3000 scans were averaged for each spectrum. Absorption and emission spectra were obtained in CH_2Cl_2. UV−vis−NIR absorption spectra were recorded on an Agilent 8453 instrument equipped with a diode array detection system. Emission spectra were measured using a JASCO FP-750 spectrofluorometer. No fluorescent contaminants were detected upon excitation in the wavelength region of experimental interest. Solutions were prepared with an absorbance between 0.1 and 0.2 at the wavelength region of experimental interest.

In recent years, density functional theory methods have become very popular. It is clear that DFT methods have many advantages; for example, they scale well with system size and implicitly include electron correlation effects and the accuracy of DFT methods is comparable to correlated ab initio procedures, such as MP2, which do not scale as well.[17] In general these methods are excellent low-cost computational procedures to analyze conjugated macromolecules in which electron correlation effect becomes a important task. Regarding their ab initio counterparts, DFT methods are also advantageous and successful in describing vibrational properties in large molecules.[18] Hence, in this work the ground-state total energies, equilibrium geometries, eigenfrequencies, and normal coordinates were calculated within the framework of density functional theory by means of the Gaussian 03 package of programs.[19] Calculations were performed using the Becke's hybrid three-parameter exchange functional (B3) combined with the nonlocal correlation functional of Lee, Yang, and Parr (LYP).[20] The Gaussian atomic basis sets 6-31G** were used.[21] Molecular orbital contours were plotted using Molekel 4.3.[22] The following constraints were assumed for the model: (i) Optimal geometries were determined on isolated entities in a vacuum. (ii) No conformational restrictions were imposed and inter-ring dihedral angles were freely rotatable. (iii) For the resulting ground-state-optimized geometries, harmonic vibrational frequencies and Raman intensities were calculated analytically and numerically, respectively. (iv) DFT calculations yield vibrational frequencies with an accuracy of about 10% compared to the respective experimental values. Calculated harmonic vibrational frequencies are uniformly scaled by a single scaling factor (0.96) to improve the numerical comparison.[23] All quoted theoretical vibrational frequencies reported are thus scaled values.

The time-dependent DFT (TD-DFT) approach is widely applied to describe electron excitations.[24] Though not as accurate for excitations as the ordinary DFT is for ground properties, the theory has considerable predictive power and is computationally quite tractable. This allows calculations for large molecules. Vertical electronic excitation energies and oscillator strengths were computed by using the TD-DFT approach. At least the 20 lowest-energy electronic excited states were computed for all the molecules. TD-DFT calculations were carried out using the same functional and basis set as in the previously optimized molecular geometries.

Acknowledgment. J.C. and G.H. are grateful to the Ministerio de Ciencia y Tecnología (MCyT) of Spain for two Ramón y Cajal Research Positions of Chemistry. This work was supported in part by the Dirección General de Enseñanza Superior (DGES, MEC, Spain) through research projects BQU2003-03194 and CTQ2004-02865-BQO. Junta de Andalucía is also thanked for funding our research group FQM-0159.

Supporting Information Available: Figure S1, showing the DFT//B3LYP/6-31G**-optimized geometries of **CH$_3$**PATfb and **F**PAMes. This material is available free of charge via Internet at http://pubs.acs.org.

References and Notes

(1) (a) Bosshard, C.; Sutter, K.; Prêtre, P.; Hulliger, J.; Flörsheimer, M.; Kaatz, P.; Günther, P. *Organic Nonlinear Optical Materials Vol. 1*; Gordon & Breach: Amsterdam, 1995. (b) Meyers, F.; Marder, S. R.; Perry, J. W. In *Chemistry of Advanced Materials: An Overview*; Interrante, L. V., Hamden-Smith, M. J., Eds.; Wiley-VCH: Weinheim, Germany, 1998.

(2) (a) Zyss, J.; Ledoux, I. *Chem. Rev.* **1994**, *94*, 77. (b) Verbiest, T.; Houbrechts, S.; Kauranen, M.; Clays, C.; Persoons, A. *J. Mater. Chem.* **1997**, *7*, 2175. (c) Alcaraz, G.; Euzenat, L.; Mongin, O.; Katan, C.; Ledoux, I.; Zyss, J.; Blanchard-Desce, M.; Vaultier, M. *Chem. Commun.* **2003**, 2766. (d) Srinivas, K.; Sitha, S.; Rao, J.; Bhanuprakash, K.; Ravikumar, K. *J. Mater. Chem.* **2006**, *16*, 496. Kang, H.; Evmeneko, G.; Dutta, P.; Clays, K.; Song, K.; Marks, T. J. *J. Am. Chem. Soc.* **2006**, *128*, 6194.

(3) (a) Lee, S. H.; Park, J. R.; Jeong, M.-Y.; Kim, H. M.; Li, S.; Song, J.; Ham, S.; Jeon, S.-J.; Cho, B. R. *Chem. Phys. Chem.* **2006**, *7*, 206. (b) Zyss, J.; Ledoux-Rak, I.; Weiss, H.-C.; Bläser, D.; Boese, R.; Thallapally, P. K.; Thalladi, V. R.; Desiraju, G. R. *Chem. Mater.* **2003**, *15*, 3036.

(4) (a) Wolff, J. J.; Siegler, F.; Matschiner, R.; Wortmann, R. *Angew. Chem., Int. Ed.* **2000**, *112*, 1494. (b) Traber, B.; Wolff, J. J.; Rominger, F.; Oeser, T.; Gleiter, R.; Goebel, M.; Wortmann, R. *Chem.*—Eur. J. **2004**, *10*, 1227. (c) Asselberghs, I.; Hennrich, G.; Clays, K. *J. Phys. Chem. A* **2006**, *110*, 6271.

(5) Hennrich, G.; Omenat, A.; Asselberghs, I.; Foerier, S.; Clays, K.; Verbiest, T.; Serrano, J. L. *Angew. Chem., Int. Ed.* **2006**, *45*, 4203.

(6) Kopelman, R.; Shortreed, M.; Shi, Y.-Y.; Tan, W.; Xu, Z.; Moore, J. S.; Bar-Haim, A.; Klafter, J. *Phys. Rev. Lett.* **1997**, *78*, 1239.

(7) (a) Gaab, K. M.; Thompson, A. L.; Xu, J.; Martínez, T. J.; Bardeen, C. J. *J. Am. Chem. Soc.* **2003**, *125*, 9288. (b) Hennrich, G.; Rurack, K.; Spieles, M. *Eur. J. Org. Chem.* **2006**, 516.

(8) (a) Thompson, A. L.; Gaab, K. M.; Xu, J.; Bardeen, C. J.; J.; Martínez, T. J. *J. Phys Chem. A* **2004**, *108*, 671. (b) Nakano, M.; Fujita, H.; Takahata, M.; Yamaguchi, K. *J. Am. Chem. Soc.* **2002**, *124*, 9648.

(9) (a) Goodson, T. G., III. *Acc. Chem. Res.* **2005**, *38*, 99. (b) Moore, J. S. *Acc. Chem. Res.* **1997**, *30*, 402. (c) Peng, Z.; Pan, Y.; Yu, B.; Zhang, J. *J. Am. Chem. Soc.* **2000**, *122*, 6619.

(10) (a) Casado, J.; Pappenfus, T. M.; Mann, K. R.; Hernández, V.; López Navarrete, J. T. *J. Chem. Phys.* **2004**, *120*, 11874. (b) Casado, J.; Ponce Ortiz, R.; López Navarrete, J. T.; Ito, S.; Morita, N. *J. Phys. Chem. B* **2004**, *108*, 18463.

(11) Long, D. A. *The Raman effect. An unified treatment of the theory of Raman Scattering by molecules*; John Wiley & Sons: Chichester, U.K., 2002. Albrecht, C. A. *J. Chem. Phys*. **1961**, *34*, 1476. Castiglioni, C.; Gussoni, M.; López Navarrete, J. T.; Zerbi, G. *Solid State Commun*. **1988**, *65*, 625.

(12) Hennrich, G.; Asselberghs, I.; Clays, K.; Persoons, A. *J. Org. Chem.* **2004**, *69*, 5077−5081.

(13) Meier, H.; Mühling, B.; Kolshorn, H. *Eur. J. Org. Chem.* **2004**, 1033. Kleinpeter, E.; Schulenburg, A. *J. Org. Chem.* **2006**, *71*, 3869. Rubin, M.; Trofimov, A.; Gevorgyan, V. *J. Am. Chem. Soc.* **2005**, *127*, 10243. Meier, H.; Muhling, B.; Oehlhof, A.; Theisinger S.; Kirsten, E. *Eur. J. Org. Chem.* **2006**, 405.

(14) For the trigonal molecules the first hyperpolarizability can be expressed by a three level model as $\beta = 1/\hbar \times \mu^2_{01}\mu_{12}/\omega_{01}{}^2 \times \omega_{01}{}^4/(\omega_{01}{}^2 - 4\omega^2)(\omega_{01}{}^2 - \omega^2)$, where μ_{01} is the transition moment between the ground and degenerate first excited charge transfer state, μ_{12} is the transition moment connecting these degenerate excited states, ω_{01} is the CT charge-transfer energy, and ω is the incident laser energy.

(15) Park, G.; Cho, B. R. *J. Phys. Org. Chem.* **2005**, *18*, 246.

(16) Myers Kelley, A.; Leng, W.; Blanchard-Desce, M. *J. Am. Chem. Soc.* **2003**, *125*, 10521.

(17) Stephens, P. J.; Devlin, F. J.; Chabalowski, F. C. F.; Frisch, M. J. *J. Phys. Chem.* **1994**, *98*, 11623. Novoa, J. J.; Sosa, C. *J. Phys. Chem.* **1995**, *99*, 15837. Casida, E.; Jamorski, C.; Casida, K. C.; Salahub, D. R. *J. Chem. Phys.* **1998**, *108*, 4439. Stratman, R. E.; Scuseria, G. E.; Frisch, M. J. *J. Chem. Phys.* **1998**, *109*, 8218.

(18) Bertsch, G. F.; Smith, A.; Yabana, K. *Phys. Rev. B* **1995**, *52*, 7876. Francl, M. M.; Pietro, W. J.; Hehre, W. J.; Binkley, J. S.; Gordon, M. S.; Defrees, D. J.; Pople, J. A. *J. Chem. Phys.* **1982**, *77*, 3654.

(19) Frisch, M. J.; et al. *Gaussian 03*, revision B.05; Gaussian, Inc.: Pittsburgh, PA, 2003.

(20) Becke, A. D. *J. Chem. Phys.* **1993**, *98*, 1372.

(21) Francl, M. M.; Pietro, W. J.; Hehre, W. J.; Binkley, J. S.; Gordon, M. S.; Defrees, D. J.; Pople, J. A. *J. Chem. Phys.* **1982**, *77*, 3654.

(22) Portmann, S.; Lüthi, H. P. *Chimia* **2000**, *54*, 766.

(23) Scott, A. P.; Radom, L. *J. Phys. Chem.* **1996**, *100*, 16502.

(24) Runge, E.; Gross, E. K. U. *Phys. Rev. Lett.* **1984**, *52*, 997. Gross, E. K. U.; Kohn, W. *Adv. Quantum Chem.* **1990**, *21*, 255. Heinze, H.; Goerling, A.; Roesch, N. *J. Chem. Phys.* **2000**, *113*, 2088.